ISSN 1990-7931, Russian Journal of Physical Chemistry B, 2024, Vol. 18, No. 4, pp. 1217–1225. © Pleiades Publishing, Ltd., 2024.

CHEMICAL PHYSICS OF NANOMATERIALS

Synthesis of Nano C60-[$Fe_3O_4/SiO_2/GeO_2$] as Efficient Catalyst Disinfection

M. Monajjemi[a], *, F. Mollaamin[b], S. Shahriari[c], and S. Mohammadi[a]

[a] *Department of Chemical Engineering, Central Tehran Branch, Islamic Azad University, Tehran, Iran*

[b] *Department of Biomedical Engineering, Faculty of Engineering and Architecture, Kastamonu University, Kastamonu, Turkey*

[c] *Department of Chemistry, Central Tehran Branch, Islamic Azad University, Tehran, Iran*

** e-mail: maj.monajjemi@iauctb.ac.ir*

Received January 14, 2024; revised March 7, 2024; accepted March 20, 2024

Abstract—The $C_{60}/Fe_3O_4/SiO_2/GeO_2$ composite was synthesized containing core/shell/shell nanomaterial by layer/layer gel method. The $C_{60}/Fe_3O_4/SiO_2/GeO_2$ composite was characterized by X-ray diffraction, field emission scanning electron microscopy fitted through scanning electron microscopy, energy dispersive X-ray spectroscopy, fourier transform infrared spectroscopy, transmission electron microscopy and UV-visible. Magnetic behavior of the synthesized product was evaluated by vibrating-sample magnetometer. The data exhibited that magnetite composites have been properly coated. This system can be applied for recycling photosensitizing way using solar energy for water disinfection. Results were reported and for degradation organic compounds via producing a single oxygen. This approach comprises C_{60} amino fullerene as a sensitizer for singlet oxygenation and $Fe_3O_4/SiO_2/GeO_2$ encapsulating magnetite nanoparticles. Fast degradation of furfuryl alcohol and methylene blue under UV-visible light exhibit that this irradiation activity of C_{60} amino fullerene-derivatives is related to the photosensitization of single oxygen. Significant single oxygen production using $C_{60}/Fe_3O_4/SiO_2/GeO_2$ system causes the effective oxidation of and inactivation of MS-2 bacteriophage under UV/visible irradiation. Our results also exhibited that the variable surfaces were effective in photo-catalyst behavior of these compounds. $C_{60}/Fe_3O_4/SiO_2/GeO_2$ composite can also be recovered and reapplied using a strong magnetic field and the photo-catalyst particles again.

Keywords: $Fe_3O_4/SiO_2/GeO_2$ composite, catalyst disinfection, core/shell nanomaterial, sol-gel method, furfuryl alcohol, methylene blue

DOI: 10.1134/S1990793124700349

1. INTRODUCTION

Electron transfer processes including nanocarbon materials such as fullerenes, nanotubes, and graphene have been investigated wildly for development of green solar-environmental and renewable energies. Fullerene photo chemically can be activated under UV/visible-light irradiation for producing singlet oxygen (O) that causes the oxidation of organic pollutants with relatively low energy [1–6]. Due to limited availability fullerene as a media photocatalyst in water strategies, the activities of C_{60} nano particles might be enhance the formation of water/C60 colloid [7], encapsulation of C_{60} in the form of micelles by surfactants [8] and surface modification of C_{60} (via hydrophilic agents) [9, 10]. Several works [11, 12] have exhibited the ability of water-soluble C_{60} including functional groups to inactivate viruses through the effective oxidation of the capsid proteins using photo chemically generated oxygen radical. Due to great susceptibility of electron-rich chemical moieties volume functionalized C_{60} nano particles achieves a fast oxidative destroying of the organic molecules under UV/visible-light irradiation [13, 14].

Nowadays, there has been large effort for providing carbon-based core-shell composite including fullerene/Fe_3O_4/SiO_2 for amazing capability in catalysis, chromatography separation, and drug delivery [15–18]. Heterogeneous photo catalysis including semiconducting dioxides such as SiO_2 and GeO_2 are an effective way to purify wastewater or gas. Magnetic properties make a suitable condition for removing and recycling magnetic composites through applying field. The mixing of C_{60}-Fe_3O_4 into GeO_2/SiO_2 matrix can block the aggregation of nanoparticles to increase the durability of the catalysts [19, 20].

In addition, these type catalysts have a high surface area and suitable pore size that enhance their photocatalyst activity; therefore, various efforts have been accomplished to develop the magnetic core-shell microspheres. Ye and Yu [21, 22] exhibited the magnetic material/SiO_2/TiO_2 composites with core-shell-shell structure through a super paramagnetic Fe_3O_4

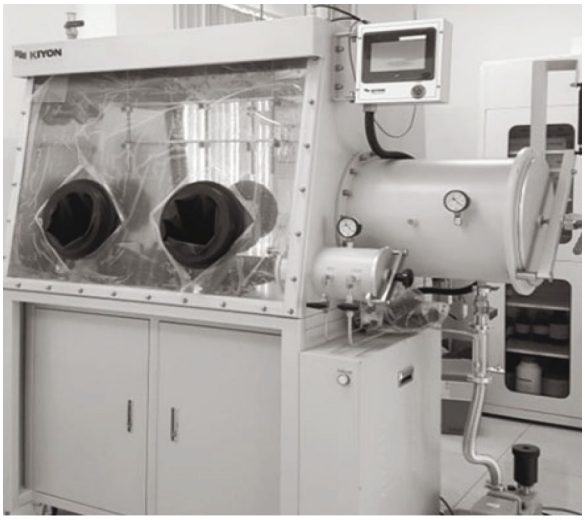

Fig. 1. The glove box model kk-011AD.

and γ-Fe_2O_3 with layers of TiO_2 through fast sol-gel mechanism and a rapid combination process [21, 22]. By this work we exhibited the GeO_2-dioxide compared with TiO_2 is more effective due to their high efficiency, good stability, availability, and nontoxicity.

2. MATERIALS AND METHOD

2.1. Purification and Preparation of Materials

Nano iron(II, III) oxide was purchased from Aldrich Chem (Germany) and Ammonia solution and CH_3-$CH(CH_3)$–CH_2OH were prepared from Merck. Tetraethoxysilane (TES) and tetrabutylzirconate (TBZ) were purchased from Tomiyama Pure Chem. Ind., Tokyo, Japan. Anhydrous ethanol was obtained from (99.9%, Aldrich Chem., Milwaukee, WI, USA). Pure Germanium dioxide was prepared from Degussa Co. Ltd and deionized water was added to all solutions in. SiO_2 was synthesized based on methods of references [23, 24]. SiO_2 gel with sizes between 0.25–0.35 micrometer was purchased from Sigma–Aldrich (Germany). 3-(triethoxysilyl) propyl succinic anhydride (TPSA) was prepared from Gelest.

2.2. Preparation of Fe_3O_4/SiO_2 Nano Spheres

The Fe_3O_4 nanomaterial (0.3 g) was high sonicated for 2 h for preparing a uniformly disperse in C_2H_5OH (60 mL). NH_4OH (4.0 mL) was added to the solution, and tetraethoxysilane (TES, $C_8H_{20}O_4Si$, Merck > 99%) TES (0.6 mL) was also added during stirring. The solution was kept stirring for 15 h. Finally, the product was affected by centrifugation for a few minutes.

2.3. Preparation of $Fe_3O_4/SiO_2/GeO_2$ Gel

The SiO_2 gel and SiO_2 fumed with mixture of $Fe_3O_4/SiO_2/GeO_2$ composites were prepared to test the photosensitizing activity of C_{60} and silica molecule was fixed for supporting the composite including 20 wt % Fe_3O_4 and 20 wt % GeO_2 nanoparticles. It should be aware that silica powder must be slowly added to the solution of $Fe(NO_3)_3{\cdot}9H_2O$ including 60 mL of C_2H_5OH during stirring. The resultant $Fe_3O_4/SiO_2/GeO_2$ Nano composites mixed by tributyltin (2 mL) and isopropyl alcohol (10 mL) drop wise and then heated at 80°C. After 12 h, the red brown precipitates were washed with deionized water and ethanol a few times and dried in a vacuum oven at 50°C for 6 h. At the end, the compounds were calcined in air at 550°C for 1 h.

2.4. Producing the 3-(2-Succinic Anhydride) Propyl Functionalized of $Fe_3O_4/SiO_2/GeO_2$ Including C_{60} as the Host Material

The gel of SiO_2/GeO_2 impregnated with Fe_3O_4 nanoparticles was tested to determine the dependence of the photosensitizing activity of C_{60} on the host compound. The Fe_3O_4 nanoparticles, SiO_2/GeO_2 powders slight by slight should be added to the solution consist of 7.35 g $Fe(NO_3)_3{\cdot}9H_2O$ including 60 mL of C_2H_5OH with slowly stirring. After the solvent was evaporated at room temperature, the product was heated to 550°C for 5 h under a flow of forming gas (5% H_2, 95% Ar) in a glove box to produce a magnetic host. Then, 2 g of magnetic powder was suspended in a binary mixture of 2 mL of TPSA and 50 mL of toluene and stirred for 20 h in glove box model kk-011AD (Fig. 1). The resultant composite was filtered, washed with toluene, and subsequently dried at 50°C, yielding 3-(2-succinic anhydride) propyl functionalized magnetic SiO_2/GeO_2 (Fig. 2).

3.RESULTS AND DISCUSSION

3.1. Scanning Electron Microscopy and Transmission Electron Microscopy Analyzing

The morphological positions of the SiO_2/GeO_2 and fullerene nano particles were studied through a transmission electron microscope (TEM) (Jeol EM-2010, JEOL Co.) and with a scanning electron microscopy (SEM) (Hitachi S-4000, Tokyo, Japan). The morphology of the composite has evaluated by emission scanning electron microscopy (FE-SEM) (Fig. 3a) indicated that the Fe_3O_4 nano magnetic particles has a diameter equal 18 ± 1 nm and due to their small size, these nanoparticles aggregation close to each other. The Pomegranate-like $Fe_3O_4/SiO_2/GeO_2$ Nano spheres with a diameter of 42 ± 1 nm are shown in Fig. 3b, that exhibited both SiO_2 and GeO_2 were successfully coated on the Fe_3O_4 nanoparticles. The images exhibited where the surfaces of

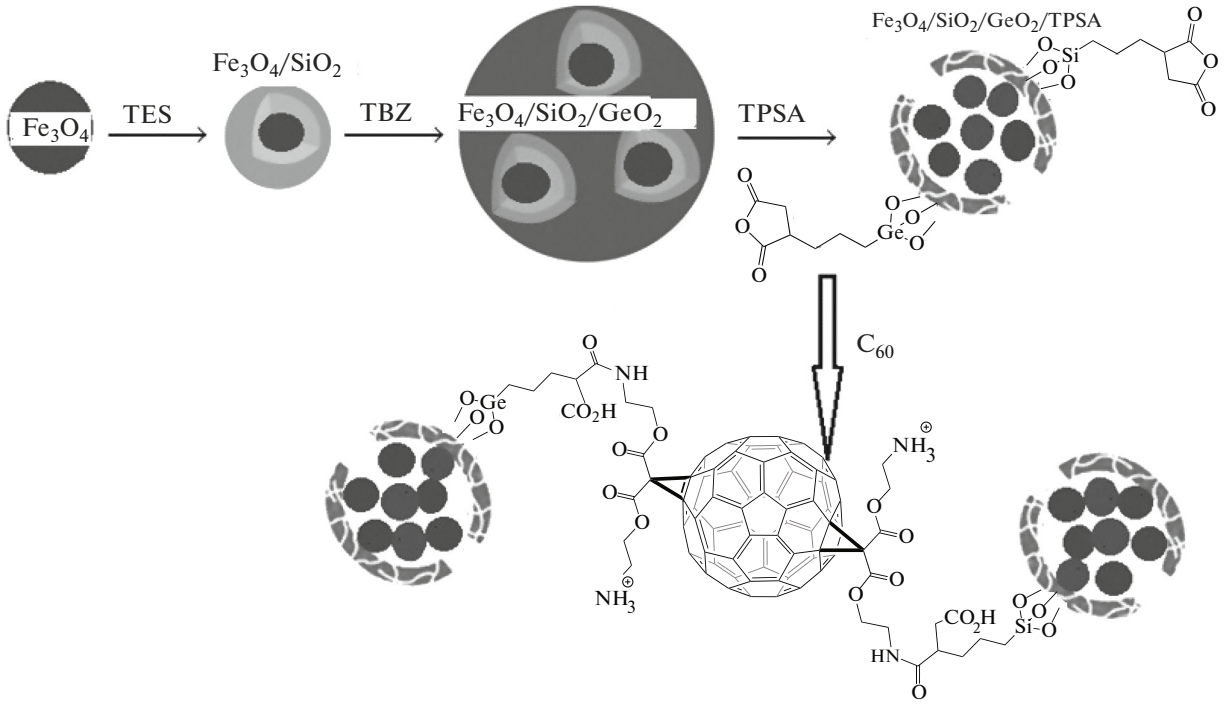

Fig. 2. The schematic process for preparing $Fe_3O_4/SiO_2/TiO_2$/TPSA composites and the Immobilization of C_{60} amino fullerene on functionalized magnetic $Fe_3O_4/SiO_2/TiO_2$/TPSA.

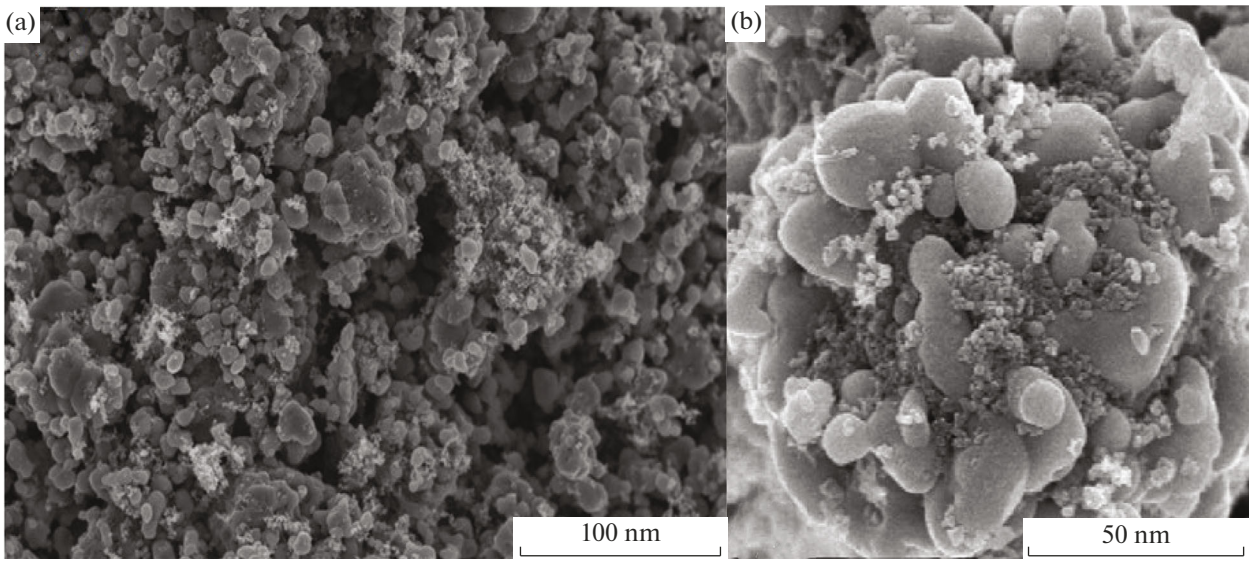

Fig. 3. (a) Fe_3O_4 nanoparticles, (b) pomegranate-llike $Fe_3O_4/SiO_2/GeO_2$ composite microspheres.

$Fe_3O_4/SiO_2/GeO_2$ microspheres are rough and porous that is suitable for the photo catalytic sensitivity.

Due to the larger radius amount of Ge compared with Si, many Fe_3O_4/SiO_2 Nano spheres are encapsulated in the core of GeO_2 shell, which can make the dyes better contact with the catalysts for degradation of these type of bio-compounds. The nanoparticle powders of products were dispersed in anhydrous C_2H_5OH by an ultrasonic water bath and then dropped onto a copper grid for TEM observation. Consequently, the

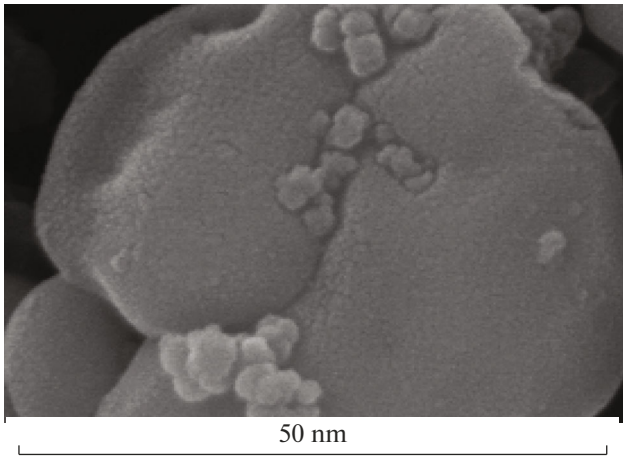

Fig. 4. TEM images of Fe_3O_4/SiO_2.

morphology of the composites also was evaluated by TEM (Fig. 4) that indicated, the Fe_3O_4/SiO_2 Nano spheres were composed of aggregated spherical particles with sizes around 24 nm.

3.2. X-Ray Diffraction Patterns

The X-ray diffraction (XRD) patterns were evaluated for the structure of hydrophilic nano particles through a PRO MPD PAN-analytical X-ray diffraction meter with a Cu anode producing X-ray generated at 45 kV and 35 mA. Fourier transform infrared (FT-IR, Bruker) spectra was fixed with wave number in the range between 450–4500 cm^{-1} and step length of 4 cm^{-1}. The magnetic behavior of the particle was measured through a vibrating sample magnetometer (VSM, Kavir Kashan Co. MDK6) at 298 K. UV-Vis absorption spectrum was also determined by a Varian Cary 5000 UV-Vis-NIR spectrophotometer. Magnetic behavior of product was characterized with a Quantum Design PPMS 6000 by metering the applied-field of magnetization between −15 to +15 kOe at 298 K. Energy dispersive X-ray spectrum (EDS, Inca Energy-200) at an accelerating voltage of 150 kV is shown in Fig. 5a. The field emission scanning electron microscopy (FESEM) fitted with EDX spectrum of $Fe_3O_4/SiO_2/GeO_2$ composite was also provided a nanostructure comprised of three main elements (Fe, Si, Ge) that confirm the $Fe_3O_4/SiO_2/GeO_2$ nanostructure formation.

The EDS that was gotten from this zone exhibited the presence of Fe, Si, Ge, and O elements. The FT-IR spectra were also recorded for three samples of (a) Fe_3O_4/SiO_2 (b) Fe_3O_4/GeO_2, (c) $Fe_3O_4/SiO_2/GeO_2$ composites without organic functional molecules (Fig. 5b). The magnetism of $Fe_3O_4/SiO_2/GeO_2$ composites was confirmed by testing in water by placing a magnet near the glass bottle. Figure 6 exhibits the X-ray diffraction (XRD) patterns of 20–70 nm for nanoparticles and core-shell of Fe_3O_4, $Fe_3O_4@SiO_2$ and $Fe_3O_4@GeO_2$ with various shell thickness. Figure 6(*1*) exhibits the XRD pattern of hydrophilic $Fe_3O_4@SiO_2/GeO_2$, and Fig. 6(*2*) and Fig. 6(*3*) are the patterns of $Fe_3O_4@SiO_2$ and $Fe_3O_4@GeO_2$, respectively at 18 nm. It is confirmed clearly that the core-shell $Fe_3O_4@GeO_2$ NPs exhibit diffraction patterns like that of $Fe_3O_4@SiO_2$. The reduction of Fe_3O_4 peaks also confirmed the successful GeO_2 coating. The as-prepared samples displayed good crystallinity;

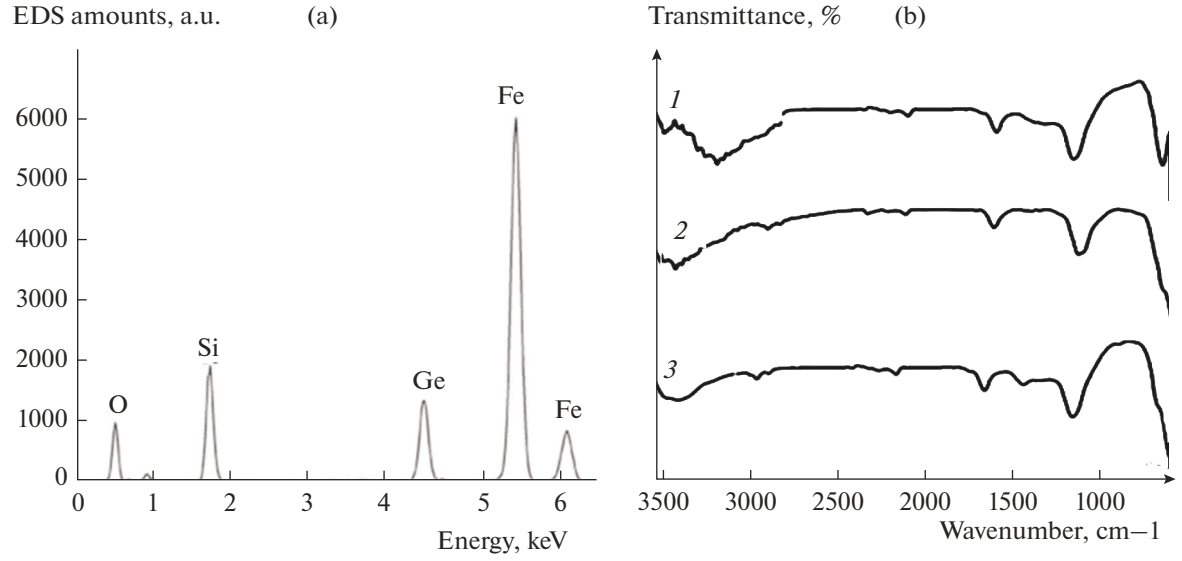

Fig. 5. (a) EDS pattern of $Fe_3O_4/SiO_2/GeO_2$ composites calcined at 550°C; (b) transmittance of IR spectra for three samples of (*1*) Fe_3O_4/SiO_2, (*2*) Fe_3O_4/GeO_2, (*3*) $Fe_3O_4/SiO_2/GeO_2$ composites.

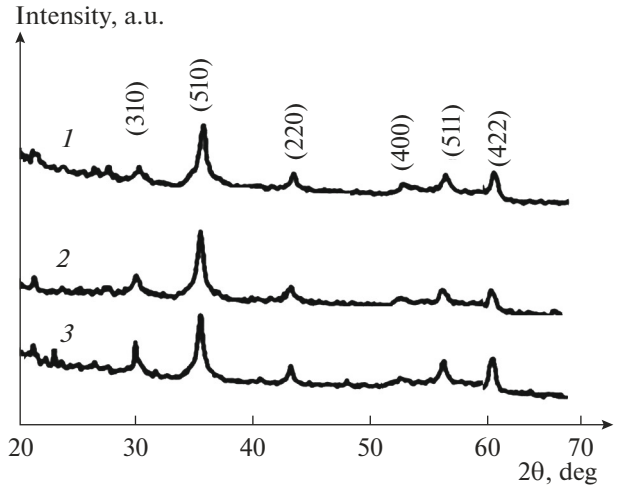

Fig. 6. XRD patterns for 2θ in the range of 20 to 70 of sample at 20–70 nm.

and the coating effect peaks can be ascribed to the (311), (440), (511), (400), and (220) planes of anatase phase (JCPDS 21-1272). According to the Scherrer equation $D = 0.\lambda 89\lambda/(\gamma\cos\theta)$ where D is the average crystallite size, the factor 0.89 is characteristic of spherical objects, is the X-ray wavelength, γ and θ are the full width at half-maximum and diffraction angle of an observed peak, respectively.

For an accurate distinguishing structure of composites, infrared spectroscopy was applied. Figure 7 exhibits FTIR spectrums of Fe_3O_4 cubes powder, Fe_3O_4/SiO_2, and $Fe_3O_4/SiO_2/GeO_2$ composites, respectively. In the FTIR spectrum of Fe_3O_4, the whole bands 1633 and 3429 cm^{-1} are tensile and flexural vibrational modes of H–O–H and confirm the water presence. Band 582 cm^{-1} exhibits the Fe–O tensile modes [25, 26].

Through comparing Figs. 6, 7 it is confirmed that asymmetric and symmetric tensile vibrational modes of Si–O–Si in 1122 and 803 cm^{-1} and flexural vibration modes of Si–O–Si have appeared in 469 cm^{-1} in the FTIR spectrum of Fe_3O_4/SiO_2 cubes nanostructures [27]. The absorption of the Ge–O bond is at 835 cm^{-1} in the FTIR spectrum of $Fe_3O_4/SiO_2/GeO_2$ cubic nanostructures [28]. The absorption of the Fe–O bond is at 495 cm^{-1} in the FTIR spectrum of $Fe_3O_4/SiO_2/GeO_2$ cubic nanostructures. By comparing the three spectra of Figs. 6, 7, the reduced frequency and the increase in the width and intensity of 1633 and 3429 cm^{-1} bands for the $Fe_3O_4/SiO_2/GeO_2$ nanostructures can be attributed to the more surface OH groups present [29]. Since surface OH groups are active sites for the adsorption, production, and decomposition of hydroxyl radical by oxidation, $Fe_3O_4/SiO_2/GeO_2$ may expose good catalytic activity to remove pollutants. According to XRD, TEM, FESEM, EDS, and FT-IR results, it could be confirmed that $Fe_3O_4/SiO_2/GeO_2$ composite with core-shell-shell nanostructured has been successfully synthesized.

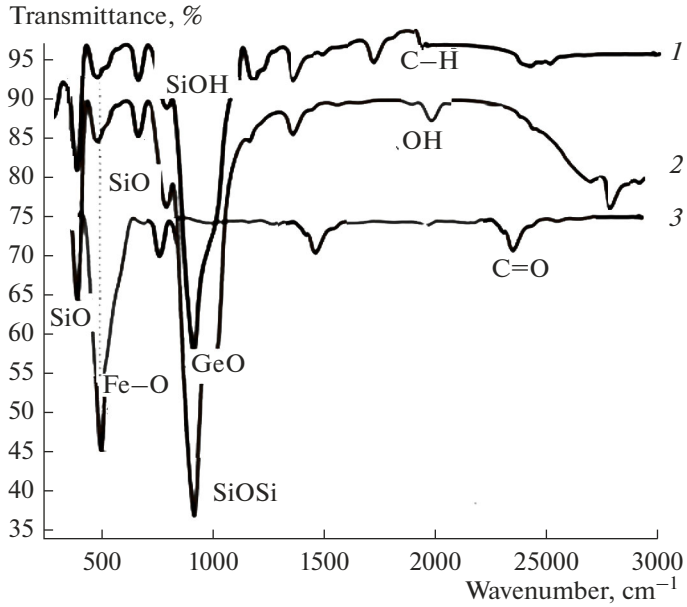

Fig. 7. FTIR spectrums of isolated bonding from mixing of $Fe_3O_4/SiO_2/GeO_2$ cubic nanostructures (a) Fe_3O_4, (b) SiO_2, and (c) GeO_2 nano particles.

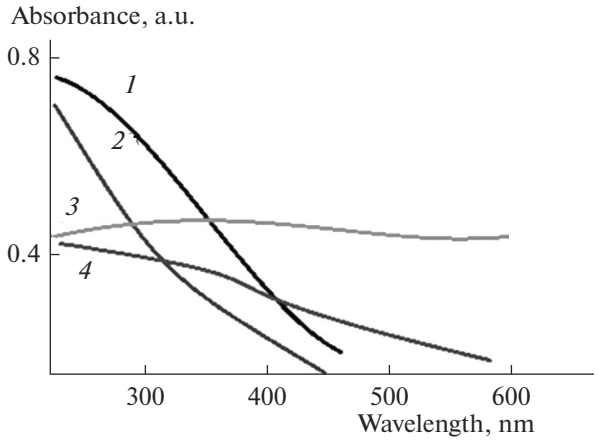

Fig. 8. UV-Vis adsorption spectra of different samples: (*1*) 20 nm hydrophilic Fe_3O_4 NPs, (*2*) 180 nm Fe_3O_4@SiO_2 core-shell NPs, (*3*) 200 nm Fe_3O_4@SiO_2 core-shell NPs, and (*4*) 220 nm Fe_3O_4@GeO_2 core-shell NPs.

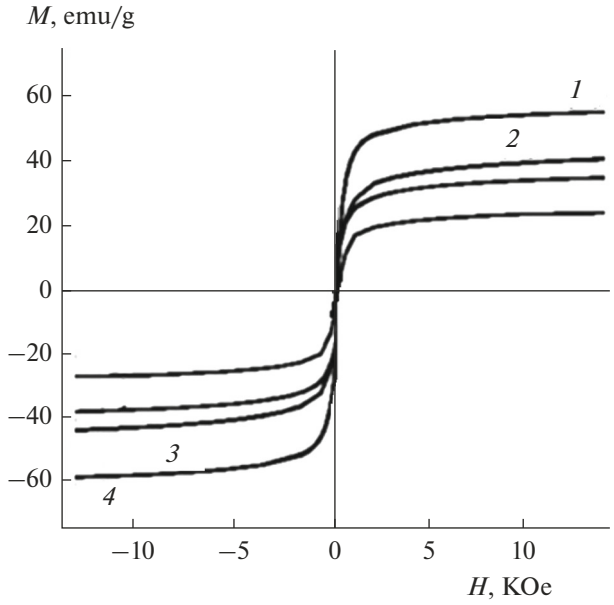

Fig. 9. Hysteresis loops at 298 K of 20 nm hydrophilic Fe_3O_4 NPs (*1*), and core-shell Fe_3O_4@SiO_2/GeO_2 including silica shell thickness of 12.0 (*2*), 15 (*3*), and 20 nm (*4*). The Ms of the 20 nm Fe3O4 NPs is about 57.0 emu g^{-1} and the Ms of the core-shell NPs are about 45, 38.0, and 26 emu g^{-1}, respectively. (Note: The Oersted (Oe) is the coherent derived unit of the auxiliary magnetic field (H) in the centimeter–gram–second system of units (CGS). It is equivalent to 1 dyne per Maxwell.)

3.3. UV-Vis Absorption

The UV-Vis absorption several composite materials are exhibited in Fig. 8 in the spectra of 20 nm Fe_3O_4 seeds and 180, 220 nm SiO_2 and GeO_2 spheres, but a broad featureless peak can be seen at a wavelength of about 378 and 388 nm in the spectrum of core-shell Fe_3O_4@SiO_2 and NPs Fe_3O_4@GeO_2. The broad peak indicated the core shell structure of the NPs and may come from the changes of band gap caused by the quantum size effect and surface effect of nanostructures and the Fe–O–Si bonds of the core-shell.

The magnetic properties of core-shell Fe_3O_4@SiO_2/GeO_2 different silica shell thicknesses were calculated using system (PPMS) at 298 K (Fig. 9). The hysteresis loops of 20 nm Fe_3O_4 NPs and Fe_3O_4@SiO_2/GeO_2 NPs with silica shell thicknesses of 12.0, 16, and 20 nm are exhibited. Figure 9(*1*) indicates the super paramagnetic property of the 20 nm nano particles, compared with the hysteresis loop of the 20.0 nm NPs, the silica coated NPs with different shell thicknesses exhibit similar magnetic properties. Figures 9(*2*), 9(*3*), and 9(*4*) exhibit the hysteresis loops of core-shell Fe_3O_4@SiO_2 NPs with silica shell thicknesses of 12.0, 16.0, and 20.0 nm, respectively.

The core-shell NPs exhibit super paramagnetic properties, as do the 20 nm Fe_3O_4 NPs. In Fig. 9(*1*) super-paramagnetic situation has been exhibited for the property of the 20 nm nano particles. It is notable, compared with the hysteresis loop of the 20 nm nano particles, the silica coated nano particles exhibit similar magnetic properties. Figures 9(*2*), 9(*3*), and 9(*4*) exhibit the hysteresis loops of core-shell Fe_3O_4@SiO_2/GeO_2 NPs with silica shell thicknesses of 12.0, 16, and 20 nm, respectively. The core-shell NPs demonstrated super-paramagnetic properties, as do the 20 nm Fe_3O_4 NPs. The Ms of Fe_3O_4@SiO_2/GeO_2 NPs with silica shell thicknesses of 12.0, 16, and 20 nm are 45, 38.0, and 26 emu g^{-1}, respectively. The decrease of Ms results from the increase of the silica component. The core-shell Fe_3O_4@SiO_2/GeO_2 NPs in dispersion responded so fast with an external magnetic field.

3.4. Photo-Catalytic Activity and C_{60} Photosensitizer

The immobilization of C_{60} amino fullerene on a magnetic silica support was accomplished according to Fig. 1 [30, 31]. An amide bridge between C_{60} amino-fullerene and succinic anhydride propyl functionalized composites were performed. The minimized coupling energies were yielded at 298 K with buffered at pH 6.5. The modified fullerene coated magnetic SiO_2/GeO_2 was extracted from the suspension. Fourier transform infrared spectroscopy patterns of the functionalized $Fe_3O_4SiO_2$/GeO_2 the surface loading of C_{60} amino-fullerene confirmed the formation of an amide bond as an organic linker based on significant peaks (Fig. 10).

$Fe_3O_4SiO_2$/GeO_2 the surface loading of C_{60} amino-fullerene based on a comparison of the UV–visible reflectance spectra of Fe_3O_4/SiO_2/GeO_2 and C_{60}/Fe_3O_4/SiO_2/GeO_2, the surface loading of C_{60} amino-fullerene increased the visible-light absorption

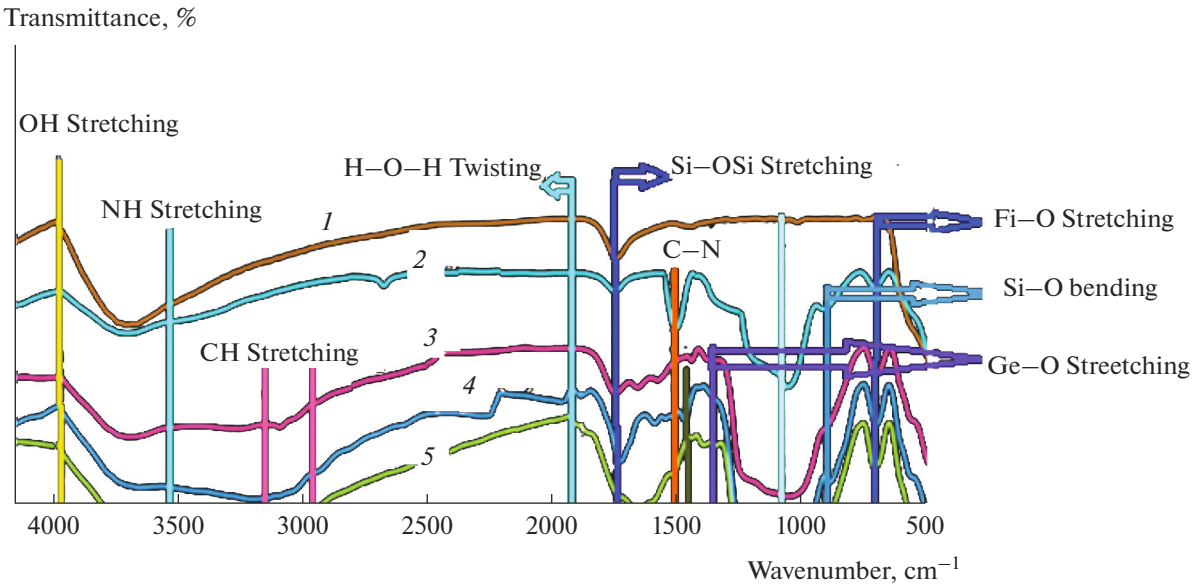

Fig. 10. Fourier transforms infrared spectroscopy (FT-IR) patterns of the functionalized.

to a slight extent. The photosensitizing activity of $C_{60}/Fe_3O_4/SiO_2/GeO_2$ system was evaluated using the degradation of furfuryl alcohol as a chemical probe [26] at the pH under visible-light irradiation.

Though a negligible furfuryl alcohol removal occurred with visible light irradiated in the absence of light, the use of $C_{60}/Fe_3O_4/SiO_2/GeO_2$ system caused a significant photochemical degradation of FFA, which implies a key role of C_{60} amino fullerene in the oxidizing capacity of magnetically separable photosensitizer composites. The photo-catalytic activity of the $Fe_3O_4/SiO_2/GeO_2$ composite materials exhibited the degradation of bio-compounds such as methylene blue by singlet oxygen in surface waters. Through adding the photo-catalytic powder of $C_{60}/Fe_3O_4/SiO_2/GeO_2$ to the methylene blue solution, nearly 60% methylene blue was degraded during UV irradiation after 1 h. Methylene blue degradation also confirms the photo-catalytic layer coating of GeO_2.

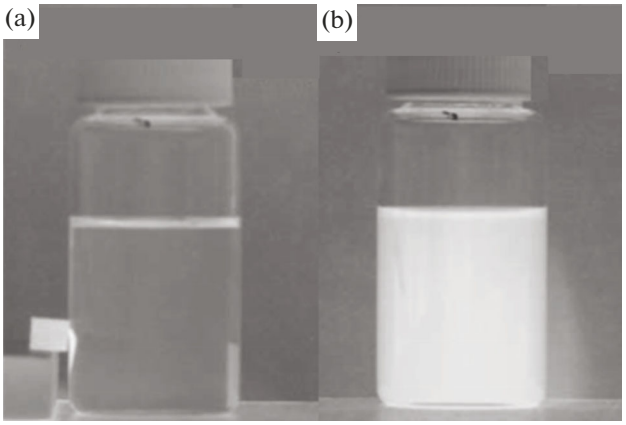

Fig. 11. Photographs of the separation and re-dispersion processes of magnetic core-shell $Fe_3O_4@SiO_2/GeO_2$ NPs: (a) with external magnetic field, and (b) without external magnetic.

3.5. Effect of Magnetic Support Types (Photographs of Nanoparticle Dispersion)

Figure 11 exhibits the photographs of the core-shell $Fe_3O_4@SiO_2/GeO_2$ nanoparticle dispersion and the response of these core-shell NPs under an external magnetic force. The 65 nm core-shell $Fe_3O_4@SiO_2/GeO_2$ NPs were dispersed in C_2H_5OH solvent of 0.6 mg mL^{-1} by sonicating for a few minutes. Through an external magnetic field, the core-shell was attracted by the magnet, leaving the ethanol solvent clear and transparent. Removing the external magnetic field and sonicating the solution re-dispersed the core-shell into the ethanol solvent, and the dispersion might be stable for a long time. The attraction and re-dispersion processes can be readily altered through applying and removing an external magnetic field, showing great potential for bio-separation. The chemical reaction can be briefly summarized as follows:

$$Si(OC_2H_5)_4 + 4H_2O/Si(OH)_4 + 4C_2H_5OH, \quad (1)$$

$$Si(OH)_4/SiO_2 + 2H_2O. \quad (2)$$

To coat SiO_2/GeO_2 onto Fe_3O_4 NPs rather than forming silica spheres, it is necessary to vary the experimental parameters to optimize the synthesis. The selectivity depends strongly on the Ostwald ripening process, and the key is to tune the competition between the nucleation and growth condensation of

SiO_2/GeO_2 [32–35]. The silica tends to coat onto the Fe_3O_4 NPs as the condensation rate is much higher than the hydrolysis rate. It was previously found that lower temperature, lower pH value, lower TEOS concentration, and less H_2O are predominant in facilitating the condensation process.

4. CONCLUSIONS

The photochemical activity of $C60/Fe_3O_4/SiO_2/GeO_2$ was examined for the oxidative degradation of organic compounds including pharmaceuticals. The kinetics for the photochemical degradation of organics is significantly dependent on the target substrate, which is attributed to the selective nature of oxygen atom as a primary oxidant in the C60-mediated photosensitizing system. The use of SiO_2/GeO_2 gel/mag and fumed SiO_2/GeO_2 as a magnetic catalyst support resulted in a drastic kinetic retardation in organic compound oxidation, which is compatible with ineffective FFA degradation.

FUNDING

This work was supported by ongoing institutional funding. No additional grants to carry out or direct this particular research were obtained.

CONFLICT OF INTEREST

The authors of this work declare that they have no conflicts of interest.

REFERENCES

1. Y. Park, N. J. Singh, K. S. Kim, et al., Chem. Eur. J. **15**, 10843 (2009). https://doi.org/10.1002/chem.200901704
2. Y. Sasada, T. Tajima, T. Wada, et al., New J. Chem. **37**, 4214–4219 (2013). https://doi.org/10.1039/C3NJ00790A
3. X. Y. Zhang, H. P. Li, X. L. Cui, et al., J. Mater. Chem. **20**, 2801 (2010). https://doi.org/10.1039/B917240H
4. J. Arbogast, A. P. Darmanyan, C. Foote, et al., J. Phys. Chem. **95** (1), 11–12 (1991). https://doi.org/10.1021/J100154A006
5. B. Vileno, A. Sienkiewicz, M. Lekka, et al., Carbon **42** (5–6), 1195–1198 (2004). https://doi.org/10.1016/j.carbon.2003.12.042
6. Y. Yamakoshi, N. Umezawa, A. Ryu, et al., J. Am. Chem. Soc. **125** (42), 12803–12809 (2003). https://doi.org/10.1021/ja0355574
7. G. V. Andrievsky, M. V. Kosevich, O. M. Vovk, et al., J. Chem. Soc., Chem. Commun. **12**, 1281–1282 (1995). https://doi.org/10.1039/C39950001281
8. A. Beeby, J. Eastoe, and R. K. Heenan, J. Chem. Soc., Chem. Commun. **2**, 173–175 (1994). https://doi.org/10.1039/C39940000173
9. J. Lee, Y. Mackeyev, M. Cho, et al., Environ. Sci. Technol. **43** (17), 6604–6610 (2009). https://doi.org/10.1021/es901501k
10. C. F. Richardson, D. I. Schuster, and S. R. Wilson, Org. Lett. **2** (8), 1011–1014 (2000). https://doi.org/10.1021/ol990312a
11. M. Cho, J. Lee, Y. Mackeyev, et al., Environ. Sci. Technol. **44** (17), 6685–6691 (2010). https://doi.org/10.1021/es1014967
12. A. R. Badireddy, E. M. Hotze, S. Chellam, et al., Environ. Sci. Technol. **41** (18), 6627–6632 (2007). https://doi.org/10.1021/es0708215
13. S. R. Chae, E. M. Hotze, and M. R. Wiesner, Environ. Sci. Technol. **43** (16), 6208–6213 (2009). https://doi.org/10.1021/es901165q
14. J. Lee, Y. Mackeyev, M. Cho, et al., Environ. Sci. Technol. **44** (24), 9488–9495 (2010). https://doi.org/10.1021/es1028475
15. F. Caruso, R. A. Caruso, and H. Mohwald, Science **282** (5391) 1111–1114 (1998). https://doi.org/10.1126/science.282.5391.111
16. R. A. Caruso, A. Susha, and F. Caruso, Chem. Mater. **13** (2), 400–409 (2001). https://doi.org/10.1021/cm001175a
17. F. Caruso, X. Shi, R. A. Caruso, et al., Adv. Mater. **13** (10), 740–744 (2001). https://doi.org/10.1002/1521-4095 (200105)13:10<740: :AID ADMA740>3.0.CO;2-6
18. G. Li, Q. Shi, S. J. Yuan, et al., Chem. Mater. **22** (4), 1309–1317 (2010). https://doi.org/10.1021/cm903501e
19. W. Cheng, K. Tang, Y. Qi, et al., J. Mater. Chem. **20** (9), 1799–1805 (2010). https://doi.org/10.1039/B919164J
20. Z. Liu, H. Bai, and D. D. Sun, New J. Chem. **35** (1), 137–140 (2011). https://doi.org/10.1039/C0NJ00593B
21. M. M. Ye, Q. Zhang, Y. X. Hu et al., Chem. Eur. J. **16** (21), 6243–6250 (2010). https://doi.org/10.1002/chem.200903516
22. X. Yu, S. Liu, and J. Yu, Appl. Catal. B **104** (1–2), 12–20 (2011). https://doi.org/10.1016/j.apcatb.2011.03.008
23. K. Y. Jung and S. B. Park, Appl. Catal. B **25** (4), 249–256 (2000). https://doi.org/10.1016/S0926-3373 (99)00134-4
24. Z. Ding, G. Q. Lu, and P. F. Greenfield, J. Phys. Chem. B **104** (19), 4815–4820 (2000). https://doi.org/10.1021/jp993819b
25. J. Zou, Y.-G. Peng, and Y.-Y. Tang, RSC Adv. **4** (19), 9693–9700 (2014). https://doi.org/10.1039/C3RA47043A
26. M. Kari, M. Montazeri-Pour, M. Rajabi, et al., J. Mater. Sci. Mater. Electron. **25** (12), 5560–5569 (2014). https://doi.org/10.1007/s10854-014-2344-x
27. V. Tizjang, M. Montazeri-Pour, M. Rajabi, et al., J. Mater. Sci. Mater. Electron. **26** (5), 3008–3019 (2015). https://doi.org/10.1007/s10854-015-2791-z

28. H. Osman, Z. Su, X. Ma, et al., Ceram. Int. **42** (8), 10237–10241 (2016). https://doi.org/10.1016/j.ceramint.2016.03.147
29. M. Montazeri-Pour and A. Ataie, Int. J. Mod. Phys. B **22** (18–19), 3144–3152 (2008). https://doi.org/10.1142/S0217979208048036
30. J. Lee, Y. Mackeyev, and M. Cho, Environ. Sci. Technol. **44** (24), 9488–9495 (2010). https://doi.org/10.1021/es1028475
31. W.R. Haag and J. Hoigne, J. Environ. Sci. Technol. **20** (4), 341–348 (1986). https://doi.org/10.1021/es00146a005
32. L. S. Chumakova, A. V. Bakulin, and S. E. Kulkova, Russ. J. Phys. Chem. B **17**, 853–859 (2023). https://doi.org/10.1134/S199079312304005X
33. A. E. Galashev, Russ. J. Phys. Chem. B **17**, 113–121 (2023). https://doi.org/10.1134/S1990793123010190
34. V. M. Kumbhar, V. M. Belekar, S. A. Jadhav, et al., Russ. J. Phys. Chem. B **17**, 222–233 (2023). https://doi.org/10.1134/S1990793123010232
35. O. S. Brovko, K. G. Bogolitsyn, I. A. Palamarchuk, et al., Russ. J. Phys. Chem. B **16**, 1204–1207 (2022). https://doi.org/10.1134/S1990793122070041